Mecánica Computacional Vol. XXI, pp. 786–804
S. R. Idelsohn, V. E. Sonzogni and A. Cardona (Eds.)
Santa Fe–Paraná, Argentina, October 2002

EXPERIMENTAL AND NUMERICAL ANALYSIS OF LOW CYCLE FATIGUE OF SPOT-WELDED JOINTS UNDER PEEL-TENSION LOADING

Alireza Gowhari-Anaraki [†], Mohammad K. Pipelzadeh [*] and Stephen J. Hardy [*]

[†] Department of Mechanical. Engineering,
Iran University of Science & Technology,
Tehran, Iran
E-mail: gohari@mech.iust.ac.ir

*School of Engineering,
University of Wales-Swansea,
Singleton Park, Swansea SA2 8PP,
United Kingdom
E-mail: m.k.pipelzadeh@swan.ac.uk
E-mail: s.j.hardy@swan.ac.uk

Keywords: Spot-welded joint, Finite element analysis, Neuber rule, Solid element model, Peel-tension loading

Abstract. *This paper investigates three different finite element models describing a single spot-welded joint of thin plates under peel-tension loading. Experimental tests have been conducted to enable comparison of the peak elastic strain measurements in the spot-weld with those predicted by the finite elements models. It was found that the solid model gives the best correlation to the strain predictions.*
The elastic-plastic finite element behaviour of the spot-welded joint under monotonic and cyclic loading is considered for two geometries. The effects of variations in post-yielding material properties on the stress and strain are considered. These results are compared with the notch-stress-strain conversion rule estimates associated with low cycle fatigue. It was found that the Neuber rule provides conservative estimates.

1 INTRODUCTION

Geometric discontinuities in engineering components such as holes, grooves, flanges, welded joints, the subject of this investigation, induce local high stresses. These are generally known as 'notches' and are likely sites for plastic formation under moderate to high loading. They are the main source of crack initiations followed by subsequent propagation and sudden failure under fatigue loading conditions. Design assessments must take account of any such stress raisers where many instances of mechanical failures can be attributed to inadequate design in the region of a discontinuity.

Spot-welded lap joints are used extensively in the fabrication of thin sheet-metal vehicle structures, such as automotive bodies and railway rolling stock. The strength of these structures is very dependent on the spot welds which are likely to be subjected to cyclic loading and may therefore fail in fatigue. Radaj[1] suggests that the hot spot stress concept, which has been successfully applied to seam-welded joints, can also be employed in the fatigue analysis of spot-welded lap joints subjected to many forms of loading. The author concludes that this method of analysis can be used to provide a suitable estimate of weld strength because the singularity in stress that occurs at the edges of the spot weld is suppressed.

Some of the research work relates to the crack propagation in the welded-joint region[2, 3] and the prediction of the fatigue life behaviour of structures containing spot-welded joints[4, 5]. The effect of geometry, loading (steady and variable), the mechanical operations such as residual stresses and various spot-weld formation methods[6] of the spot-welded joint were investigated in order to increase the fatigue strength.

Finite element analysis is a powerful tool used by the designer to predict the behaviour of structures such as those mentioned above. In this case, an effective representation of the spot welds is necessary in order to provide the continuity between plates while, at the same time, ensuring that realistic stresses around the edges of the nugget are predicted. A number of spot weld models have been proposed and investigated and their suitability discussed. Sheppard and Strange[7] introduced six finite element models for a spot-welded joint and have discussed the attributes, but not the accuracy, of each model. Forrest et al[8] have modelled spot-welded plates using solid brick elements with the nodes at the weld nugget being merged. This technique is not appropriate for analysing vehicle body designs because they are normally constructed from thin plates. They used four different models for a single spot-welded joint but have not presented any detailed information on their performance. Pal and Cronin[9] have studied experimental and finite element analyses of three representative cross-sectioned box beams under static and dynamic bending and torsion loading. Both the rigid bar and elastic rod models representing the spot-weld were significantly in error. However, for the finite element model that consists of six-sided solid elements with eight grid points as the nugget and quadrilateral plate elements for the plates, the predictions were within 10% of the experimental static deformation results. Rui et al[10] have used beam elements as the weld nugget, which is common in vehicle body analysis.

In the present study, three different methods of modelling spot welds are compared for a

single spot lap joint subjected to peel-tension loading. This form of loading is most likely to cause failure by fatigue (either high or low cycle)[7,11, 12, 13]. The effects of plate width, length and thickness and spot diameter on the elastic stress concentration factor (SCF) are investigated. These are based on a solid model for a range of geometric dimensions. In addition, an experimental investigation was conducted using two spot-weld geometries under peel-tension loading using stain gauges in order to validate the predictions from the finite element models. A typical geometry with relatively moderate SCF is selected to study the elastic-plastic behaviour of the spot-weld joint. Below the yield stress of the material, there is a direct relationship between the maximum stress, σ_{max}, at the notch root and the nominal stress applied remotely from the notch region, σ_a. Their ratio (i.e., σ_{max}/σ_a) is referred to as the SCF, K_t. These are both geometry and loading dependent and are particularly useful for brittle materials in order to predict the peak stresses. However, for post yielding, the local regions of high stress are relieved as yielding occurs and results in the formation of plastic zone. σ_{max} will no longer become equal to (σ_a K_t). Therefore, the SCF is not appropriate and a criterion based on the accumulation of strain is more relevant and can be used to assess the low cycle fatigue behaviour. Finite element method is expensive and time consuming. Alternatively, simple numerical relationships have been proposed. These are known as notch stress-strain conversion (NSSC) rule estimates. Typically Neuber[13], Hardrath-Ohman[14], Linear and the intermediate rules[15] are used to estimate the strain values.

2 NOTATION

d	Spot-weld mean diameter
E	Elastic modulus
E_{eff}	Effective elastic modulus
F	Applied tensile load
I	Second moment of area of the plate across the spot-weld region
K_ε	Meridional geometric strain concentration factor
K_σ	Meridional geometric stress concentration factor
K_t	Elastic stress concentration factor
L	Plate length
m	Index
M	Bending moment
t	Plate thickness
W	Plate width (Distance between two consecutive weld-spots)
α	Ratio of (E/E_{eff})
β	Strain hardening parameter
ε	Strain
$\hat{\varepsilon}$	Maximum strain
λ	Nominal loading parameter
σ	Stress
$\hat{\sigma}$	Maximum stress

υ Poisson's ratio

2.1 Subscripts

a Nominal
eq Equivalent
m Meridional
max Maximum
y Yield

3 NOTCH STRESS-STRAIN CONVERSION RULES

Components subjected to intermediate and low cycle fatigue will experience large yielding. In these regions, the plastic stress concentration factor, K_σ and the elastic-plastic strain concentration factor, K_ε are no longer equal to the geometry elastic stress concentration factor, K_t. Many researchers have investigated the relationships between these factors. These are known as the notch stress-strain conversion, NSSC, rule estimates. For two-dimensional problems (e.g., plane stress situation, such as thin plates), the Neuber rule[13] is found to give a good estimate. The linear rule is normally associated with plane strain situations (e.g., thick plate). For three-dimensional problems or axisymmetric components, the intermediate rule has been considered since it lies between these two extreme cases.

For the Neuber rule under uniaxial loading, the correlation of the above concentration factors are found to be:

$$K_\sigma K_\varepsilon = \frac{\hat{\sigma}\hat{\varepsilon}}{\sigma_a \varepsilon_a} = K_t^2 \qquad (1)$$

Hence, for monotonic loading:

$$\hat{\sigma}\hat{\varepsilon} = K_t^2 \, \sigma_a \varepsilon_a \qquad (2)$$

and for cyclic loading:

$$\Delta\hat{\sigma}\,\Delta\hat{\varepsilon} = K_t^2 \, \Delta\sigma_a \Delta\varepsilon_a \qquad (3)$$

where $\hat{\sigma}$, $\hat{\varepsilon}$ are peak stress and strain at the notch respectively and σ_a , ε_a are nominal stress and strain measured remotely from the notch. 'Δ' refers to the range (i.e., peak to peak change during a cycle).

For the intermediate rule[15], the relationship between K_σ K_ε and K_t is expressed by:

$$K_\varepsilon / K_t = (K_t / K_\sigma)^m \qquad (4)$$

$$m = \frac{\log(K_\varepsilon / K_t)}{\log(K_t / K_\sigma)} \qquad (5)$$

When index 'm' is set equal to 1, it will correspond to the Neuber rule (see Equation 1). However, for m=0, it gives the other extreme condition, which is the Linear rule (i.e., K_ε =

K_t).

The above rules can be modified further to include the effect of multi-axial states-of-stress using various methods[16]. For these components, although the meridional stress (i.e., parallel to the surface) is the dominant stress, the hoop and radial stresses cannot be ignored. Therefore, Equation 1 can be expressed in terms of meridional and equivalent stress and strain components as follows: considering a tri-axial states-of stress in the meridional direction (e.g., denoted by x):

$$\frac{\sigma_x}{\varepsilon_x} = \frac{E}{\left\{1-\nu\left(\frac{\sigma_y}{\sigma_x}+\frac{\sigma_z}{\sigma_x}\right)\right\}} = E_{eff} \qquad (6)$$

or

$$\alpha = \frac{E}{E_{eff}} = 1-\nu\left(\frac{\sigma_y}{\sigma_x}+\frac{\sigma_z}{\sigma_x}\right) \qquad (7)$$

Hence, the Neuber rule becomes:

$$K_\sigma K_\varepsilon = \alpha K_t^2 \qquad (8)$$

And the intermediate rule is:

$$K_\varepsilon / \alpha K_t = (K_t / K_\sigma)^m \qquad (9)$$

$$m = \frac{\log(K_\varepsilon / \alpha K_t)}{\log(K_t / K_\sigma)} \qquad (10)$$

where,

$$K_\sigma = \frac{\hat{\sigma}_m}{\sigma_a}\ ,\ K_\varepsilon = \frac{\hat{\varepsilon}_m}{\varepsilon_a} \qquad \text{(monotonic loading)}$$

$$K_\sigma = \frac{\Delta\hat{\sigma}_m}{\Delta\sigma_a}\ ,\ K_\varepsilon = \frac{\Delta\hat{\varepsilon}_m}{\Delta\varepsilon_a} \qquad \text{(cyclic loading)}$$

The subscript ‘m’ refers to the meridional direction and K_t is the maximum meridional stress index, $\hat{I}_m$.

For equivalent values of stress and strain, the term ‘α’ is set equal to 1. Therefore:

$$K_\sigma = \frac{\hat{\sigma}_{eq}}{\sigma_a}\ ,\ K_\varepsilon = \frac{\hat{\varepsilon}_{eq}}{\varepsilon_a} \qquad \text{(monotonic loading)}$$

$$K_\sigma = \frac{\Delta\hat{\sigma}_{eq}}{\Delta\sigma_a}\ ,\ K_\varepsilon = \frac{\Delta\hat{\varepsilon}_{eq}}{\Delta\varepsilon_a} \qquad \text{(cyclic loading)}$$

where the subscript 'eq' refers to the von-Mises equivalent stress and strain and K_t is the maximum equivalent stress index, $\hat{I}_{eq}$.

4 GEOMETRIES

The basic arrangement of the peel-tension loading component is made from two 'L' shaped plates joint together with their common bases to form a 'T' shaped component using a single spot weld at the centre, as shown in Figure 1. The geometry of the spot-welded joint is described by four dimensions, the plate length, L, the plate width, w, the plate thickness, t and spot-weld diameter, d. In this study, two non-dimensional parameters are considered by

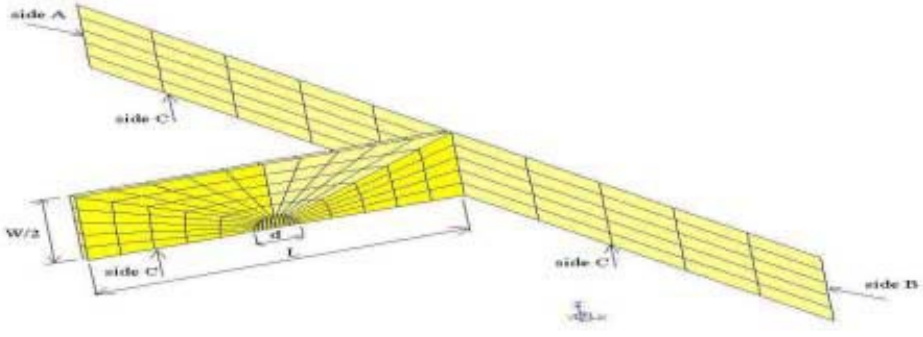

Figure notation:
Side A: Equal point loads applied to the surface
Side B: Displacement and rotational constraints are applied to the surface in X, Y and Z directions
Sides C: Line of symmetry of the component (Contrained in Z direction)
A constant thickness, t, is considered for all plates.

Figure 1: A typical finite element half model of the spot-welded joint with geometric dimensions and applied load and constraints.

normalising with respect to the spot-weld diameter, d. These are t/d and w/d. The effect of geometric parameter L/W is also considered. The thickness of the plate is small compared to the other dimensions.

For the elastic-plastic analysis, a typical geometry with a moderate stress concentration is considered. The component geometric dimensions are L/W=1.7, W/d=0.2 and t/d=0.2.

5 LOADING AND BOUNDARY CONDITIONS

Figure 1 shows a typical mesh of a half of the model with loading and boundary conditions.

A uniform eccentric tensile load is applied to one free end of the plates and reacted by constraining the other end of the plate in all directions (i.e. displacement and rotation). For peel-tension loading, the welded joint is subjected to greater stresses compared to the other welded joints[1, 17]. This is mainly caused by the bending stresses. The elastic SCF can be obtained as follows:

$$K_t = \frac{\sigma_{max}}{\sigma_a} \qquad (11)$$

where σ_{max} is the maximum stress at the weld nugget and σ_a, is the nominal bending stress in the plate defined as follows:

$$\sigma_a = \frac{Mc}{I} \qquad (12)$$

where: c= t/2
I= (1/12) (W-d) t^3
and M= F . (L/2)
F= is the applied eccentric tensile load
(L/2) is the perpendicular distance from the applied load to the centre of the spot-weld.

For the elastic-plastic analysis, the magnitude of the applied tensile load is described in terms of a non-dimensional tensile loading parameter, λ, where:

$$\lambda=\sigma_a/\sigma_y \qquad (13)$$

where σ_y is the yield stress of the material.

6 FINITE ELEMENT ANALYSIS

Finite element predictions of the spot-weld are obtained using the standard linear and non-linear codes of NISA suite of programs[18]. Throughout the analyses, four-sided, eight-noded isoparmateric elements were used to represent the plates as shown in Figure 1. However, the weld nugget region has been modelled using the following three methods:

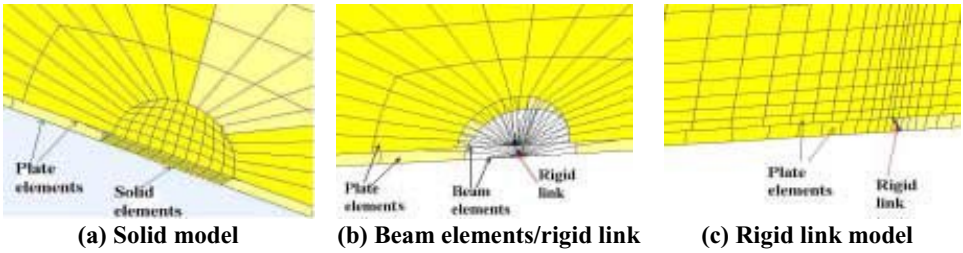

(a) Solid model **(b) Beam elements/rigid link** **(c) Rigid link model**

Figure 2: Finite element models considered for the spot-weld.

Method 1- 3D solid elements with six-sided, eight-noded isoparmeteric elements were used with a 2 by 2 by 2 integral Gauss array of as shown in Figure 2(a)). This model was chosen

because of the good agreement found with experimental results[9].

Method 2- beam elements with diameter equal to that of the weld nugget (spoke shaped) and one rigid link model (see Figure 2(b)). This model was chosen because it is similar to the actual nugget and because it is easy to use.

Method 3- one rigid link element as shown in Figure 2(c). Again, this model is easy to develop and is very often used in finite element analyses of spot-welded vehicle structures.

The elastic-plastic stress-strain behaviour of the spot-welded joint material is modelled throughout using a simplified linear elastic-linear strain hardening, time-independent, material model. The degree of strain hardening, referred as β, expressed by the ratio of plastic to elastic modulus (i.e., $\beta = E_p/E$), varies from $\beta=0$ (i.e. elastic-perfectly-plastic) to $\beta=1$ (i.e. perfectly elastic). For cyclic loading, the elastic-perfectly-plastic (EPP), and elastic-kinematic-hardening (EKH) models are used to describe the material behaviour with β values ranging from 0 to 0.2. These are typical values for ferrous and non-ferrous engineering materials. The von-Mises effective stress criterion and the associated Prandtl-Reuss flow rules were used for the multiaxial elastic-plastic behaviour. Values for Young's modulus, uniaxial initial yield stress and Poisson's ratio of 209 GPa, 100 MPa and 0.3 respectively were used throughout the analysis. The results are normalised with respect to material properties and therefore can be applied to geometrically similar components made from other materials.

7 MONOTONIC TESTING OF THE PEEL-TENSION LOADING

Experiments were performed in order to compare the measured strain with the prediction from the three finite element models described in the previous section. The samples conform to DIN 50124 standards and are made from ST. 1203 sheets. Two experimental geometries are considered. The geometric dimensions of the specimens are shown in Table 1.

Geometry*	L	W	d	T
1	38	50	7	1.5
2	38	75	7	1.25

* All dimensions are in mm

Table 1: Geometric dimensions of tested specimens.

For the peel-tension loading, a bi-axial strain gauge was employed for the measurement of the strain in the vicinity of the spot-weld. This is positioned at the external face of the plate close to and normal to the radius of the spot weld. The size of the strain gauge must be greater than both the thickness of the plate and diameter of the spot weld. The measured strain is the average strain under the area covered by the strain gauge which is dependent on the dimension of the strain gauge and the distance from the tip of the weld. Therefore, the measured strain is

always slightly lower than the actual peak strain.

The samples were placed on a 25 Tonne tensile test machine with grip lengths of 40 mm. The strain gauge is connected to a strain indictor. For each geometry, the applied force against the strain reading is recorded for the load range of 0 to 0.35 KN.

8 RESULTS

8.1 Experimental and finite element results

Figures 3(a) and 3(b) show the variations of strain readings in the X and Y-directions

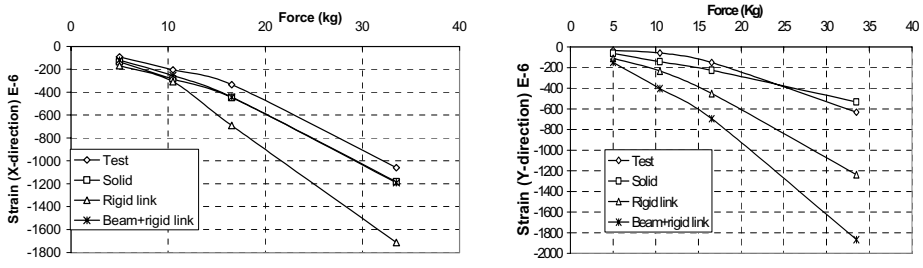

(a) X-direction **(b) Y-direction**

Figure 3: Variation of strain distributions with applied tension peel force for the experiment and finite element models for Geometry 1 in (a) X-direction and (b) Y-direction.

respectively against the applied peel-tension loading for Geometry 1. Similarly, the above variations for Geometry 2 are shown in Figure 4. It is clearly evident that the both the solid element and beam/rigid link models predictions are in good agreement with the experimental

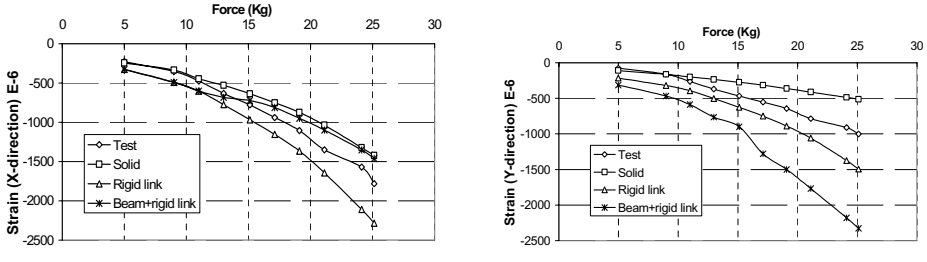

(a) X-direction **(b) Y-direction**

Figure 4: Variation of strain distributions with applied tension peel force for the experiment and finite element models for Geometry 2 in (a) X-direction and (b) Y-direction.

results in the X-direction. However, in the direction, the discrepancy increases significantly, in

particular for the beam/rigid link model. The solid model gives a maximum discrepancy of $\pm$15% and therefore provides a better estimate for the single spot-weld joints compared to the other models. The overall results show that the level of discrepancy increases as the applied load increases in particular for beam/rigid link and the rigid link models.

8.2 Comparisons of spot-weld finite element models

From the experimental results, the solid model was found to reasonably represent the behaviour of the spot-welded joint. This model will be used to obtain the SCF data for the

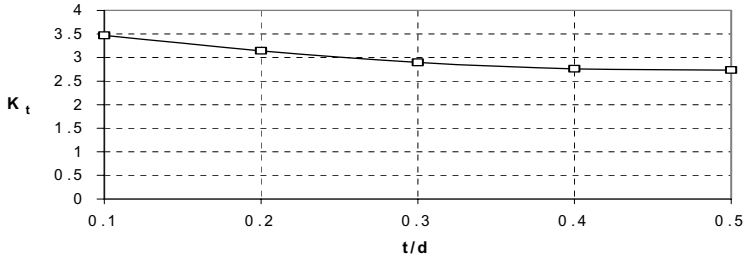

Figure 5: Variation of elastic stress concentration factor, K_t with t/d for L/W=1 and L/d=5.

range of geometric parameters. Both the beam/rigid link and rigid link models predict values of K_t, greater than the corresponding values with the solid elements (as was the case for the experiment). A similar effect was identified by Radaj[1] using "spoked star model" where rigid spokes provided higher SFC predictions than soft (elastic) spokes.

8.3 Elastic finite element analysis

The results from the parametric studies using the solid model are presented in Figures 5 to

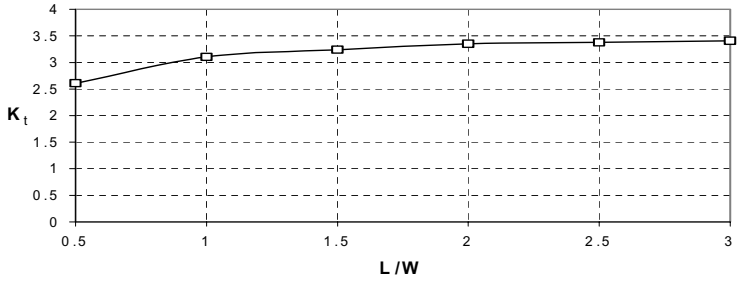

Figure 6: Variation of elastic stress concentration factor, K_t with L/W for W/d=5 and t/d=0.2

7 for the elastic SCF, K_t. These are obtained from Equation 11. The effect of varying the thickness of the plates on K_t is shown in Figure 5 for a constant diameter, d and for L/W = 1

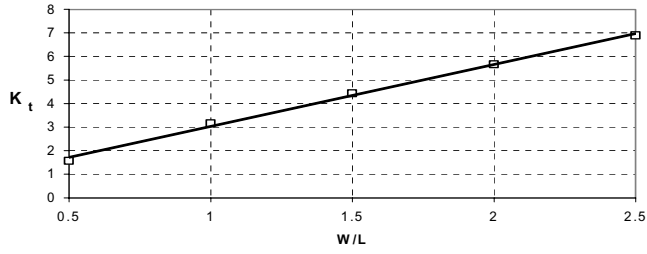

Figure 7: Variation of elastic stress concentration factor, K_t with W/L for L/d=5 and t/d=0.2

and L/d=5. It clearly shows that increasing the thickness results in the slight reduction in K_t value. K_t becomes virtually independent of t/d for t/d > 0.4. In contrast, K_t increases with an increase in the length of the plates, L, as shown in Figure 6 for a constant W and for W/d=5 and t/d=0.2. Again, K_t becomes virtually independent of L/W for L/W > 2.5. The effect of the variation of width of the plates, W, on K_t for a constant L and for L/d=5 and t/d=0.2 can be seen in Figure 7. A linear relationship is obtained which can be expressed by:

$$K_t = 2.63\ W/L + 0.41 \qquad (14)$$

8.4 Elastic-plastic finite element analysis

8.4.1 Monotonic loading

Maximum meridional stress and strain are taken at the worst Gauss point in the spot-weld region and normal to the direction of the applied load. This was found to be the dominant component. The effect of the tri-axial state-of-stress obtained in a form of equivalent stress and strain is found to be insignificant. All the results are given in a form of normalized stresses and strains. These are obtained by dividing the predicted stress or strain values by the corresponding nominal values, i.e.

For the meridional direction:

Normalized meridional stress= σ_m/σ_a

Normalized meridional total strain= $\varepsilon^t_m/\varepsilon_a$

For equivalent values:

Normalized equivalent stress= σ_{eq}/σ_a

Normalized equivalent total strain= $\varepsilon^t_{eq}/\varepsilon_a$

8.4.1.1 Effect of nominal load parameter, λ

The effect of the variation of nominal load parameter, λ, on the maximum normalized

meridional and equivalent stress and total strain can be seen in Figure 8 respectively. The main features of the overall behaviour are as follows:

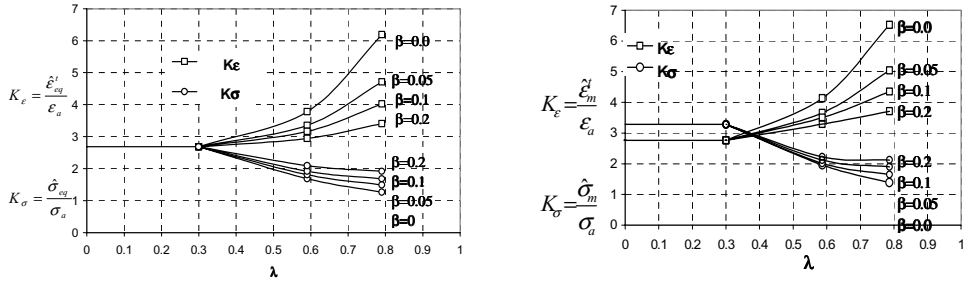

(a) Equivalent **(b) Meridional**

Figure 8: Variation of (a) $\hat{\sigma}_{eq}/\sigma_a$ and $\hat{\varepsilon}^t_{eq}/\varepsilon_a$ and (b) $\hat{\sigma}_m/\sigma_a$ and $\hat{\varepsilon}^t_m/\varepsilon_a$ with β and λ under monotonic loading conditions.

(1) The onset of tensile yielding is found to occur when the monotonic nominal load, λ, becomes equal to 0.3. Below this value, the behaviour of the component is purely elastic. Both normalized equivalent stress, K_σ and normalized equivalent total strain, K_ε remain equal to geometric elastic stress concentration factor, K_t. However there is a slight difference between the normalized meridional stress, and meridional total strain components. This is mainly caused by the tri-axial effect of the other stress tensors.

(2) It is clearly evident that further increase in the monotonic nominal load, λ, will result in an increase in normalized total strain coupled with the corresponding reduction in the stress component.

8.4.1.2 Effect of material hardening

Figure 8 also includes results for material hardening with β> 0. The main features are summarized as follows:

The onset of the tensile yielding remains the same for all material models and below this value, the material behaviour is purely elastic.

Above yielding, increasing the degree of strain hardening will result in increase in stresses accompanied by a reduction in the strains. The extent of plastic propagation in the yielded regions reduces as β increases (i.e. for β=1, there is no plastic deformation).

8.4.2 Repeated tensile loading

For the repeated loading condition (i.e., loading and unloading), results are presented in the form of normalized meridional stress and strain ranges. These are obtained by dividing the predicted stress and strain ranges by the corresponding nominal values in the plates, i.e.,

For the meridional direction:

Normalized meridional stress range= $\Delta\sigma_m/\Delta\sigma_a$

Normalized meridional total strain range= $\Delta\varepsilon^{t}_{m}/\Delta\varepsilon_a$

For equivalent values:

Normalized equivalent stress range= $\Delta\sigma_{eq}/\Delta\sigma_a$

Normalized equivalent total strain range= $\Delta\varepsilon^{t}_{eq}/\Delta\varepsilon_a$

The unloading condition will result is a residual stress and strain, the extent of which can be categorized by one of the following situations:

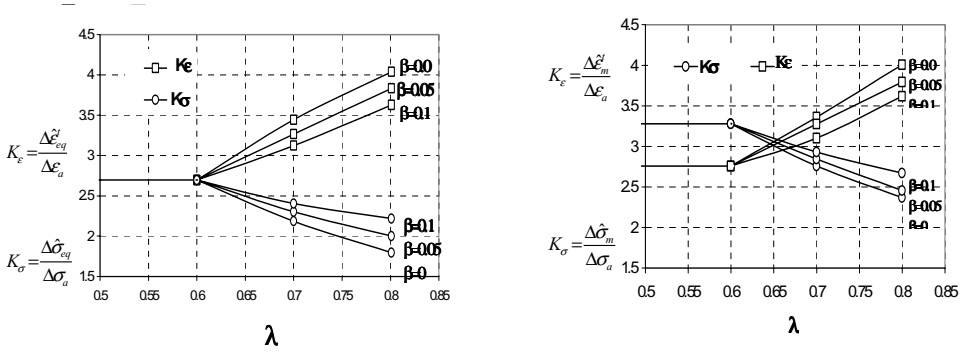

Figure 9: Variation of (a) $\Delta\hat{\sigma}_{eq}/\Delta\sigma_a$ and $\Delta\hat{\varepsilon}^{t}_{eq}/\Delta\varepsilon_a$ and (b) $\Delta\hat{\sigma}_{m}/\Delta\sigma_a$ and $\Delta\hat{\varepsilon}^{t}_{m}/\Delta\varepsilon_a$ with β and λ under repeated loading conditions.

(1) For loading conditions within the elastic range, the loading and unloading is purely elastic, i.e. the elastic limit is for λ = 0.6.

(2) Increasing λ above the yield point will produce a loading cycle which consists of tensile yielding during loading and elastic unloading. Under these conditions, normalized stress and strain ranges remain constant and equal to their respective elastic stress and strain concentration factors.

(3) Further increases in λ will result in tensile yielding, elastic unloading and compressive yielding upon unloading. The latter condition will form a compressive plastic strain which is defined by a reversal in the direction of plastic straining[19].

Throughout the analysis, a steady-state strain response is achieved after the completion of the first cycle using the EPP and EKH material models.

8.4.2.1 Effect of nominal load parameter, λ

The variation of maximum normalized meridional and equivalent stress range and total strain range with load parameter, λ, for various material hardening, β, can be seen in Figures 9(a) and 9(b) respectively. The overall effect of λ on the behaviour of spot-welded joints under repeated loading is similar to those described for the monotonic loading case. However, the onset of compressive yielding occurs when nominal load, λ, becomes equal to 0.6. This is

twice the magnitude of the corresponding monotonic loading.

8.4.2.2 Effect of material hardening, β

The effects of β on the stress and strain ranges can also be seen in Figure 9. These are summarised as follow:

(1) The stress and strain ranges remain within the elastic limit upon unloading for λ value less than 0.6. Both EPP and EKH hardening models will give identical results.

(2) Above the reverse yielding limit, increasing the degree of strain hardening will result in an increase in stresses coupled with a reduction in the strains. The overall stress and strain range predictions are less than for the monotonic loading condition for all λ values.

8.5 Comparison of finite element predictions with NSSC rule estimates

In this section, the predicted finite element total strain ranges for a variety of monotonic and cyclic loads and material hardening models are compared with values obtained from

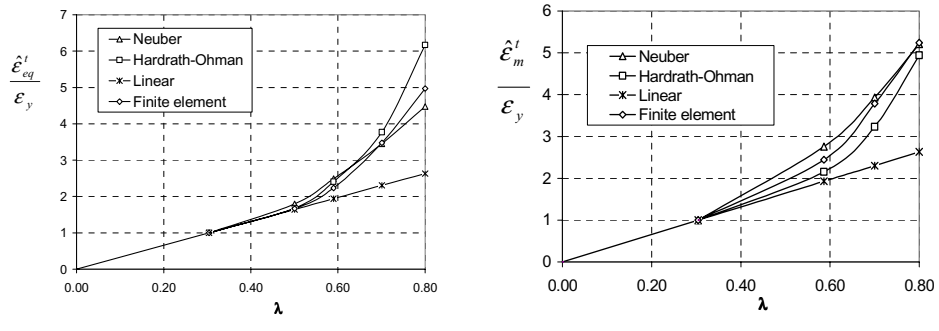

Figure 10: Comparison between finite element predictions of maximum (a) equivalent total strain and (b) meridional total strain and simple NSSC rule estimates under monotonic loading with an EPP model.

simple NSSC rule estimates. For monotonic loading, the strain range is taken as the strain at full load. For cyclic loading and EPP and EKH models, a stable loop, with a steady strain range is predicted after the first cycle. Tables 2 and 3 list the derived 'm' values for monotonic and repeated loading respectively which are based on the intermediate rule. These are obtained from Equations 5 and 10. The derived 'm' values range from 0.37 to1.50 with an overall average value of 0.92. Maximum equivalent and meridional strain predictions with an EPP material model are compared with the simple NSSC rule estimates, using the equations outlined in section 3, in Figures 10 and 11 for monotonic and repeated loading conditions. Again, for all loading considered, the linear rule represents the lowest limit and the upper limit is dependent on the magnitude and loading condition. The Neuber rule and to less extent, Hardrath-Ohman rule provided the upper bound. Therefore, fatigue life predictions based on

strain range estimates using the Neuber rule will be conservative.

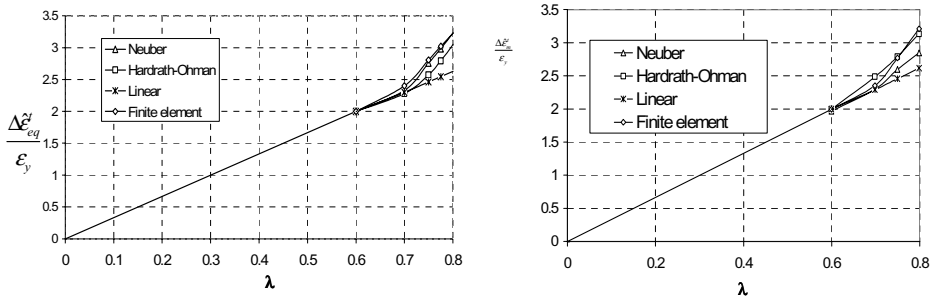

(a Equivalent **(b)Meridional**

Figure 11: Comparison between finite element predictions of maximum (a) equivalent total strain range and (b) meridional total strain range and simple NSSC rule estimates under repeated loading with an EPP model.

Index 'm'				
Loading parameter 'λ'	**Material hardening 'β'**			
	β=0	**β=0.05**	**β=0.10**	**β=0.20**
0.6	0.74 (0.79)	0.57 (0.58)	0.49 (0.54)	0.37 (0.45)
0.8	1.10 (0.99)	0.96 (0.87)	0.86 (0.83)	0.71 (0.68)

Values in brackets are meridional 'm' values

Table 2: Derived 'm' values for the intermediate NSSC rule based on finite element predictions of equivalent and meridional stress and strain under monotonic peel-tension loading.

A typical sample of calculations with $\lambda = 0.8$ and an EPP material model is illustrated below:

(1) **Monotonic loading**

The elastic equivalent stress, meridional stress and total strain concentration factors of $K_{teq}= 2.7$, $K_{t\sigma}= 2.76$ and $K_{tm}= 3.28$ respectively are taken from Figure 8.

Index 'm'			
Loading parameter 'λ'	**Material hardening 'β'**		
	β=0	**β=0.05**	**β=0.10**
0.70	1.15 (1.14)	1.19 (1.20)	1.26 (1.04)
0.80	1.00 (1.15)	1.17 (1.10)	1.50 (1.32)

Values in brackets are meridional 'm' values

Table 3: Derived 'm' values for the intermediate NSSC rule based on finite element predictions of equivalent and meridional stress and strain range under repeated peel-tension loading.

Also, from the elastic-plastic analysis, and from Figure 8:

$K_{\sigma eq} = \hat{\sigma}_{eq} / \sigma_a = 1.27$, $K_{\varepsilon eq} = \hat{\varepsilon}^t_{eq} / \varepsilon_a = 6.19$

$K_{\sigma m} = \hat{\sigma}_m / \sigma_a = 1.38$, $K_{\varepsilon m} = \hat{\varepsilon}^t_m / \varepsilon_a = 6.52$

For meridional stress and strain using Equation 10:

$$m = \frac{\log(K_{\varepsilon m} / \alpha K_{tm})}{\log(K_{tm} / K_{\sigma m})}$$

where $\alpha K_{tm} = K_{tm}$

thus m= 0.99

For equivalent stress and strain using Equation 5:

$$m = \frac{\log(K_{\varepsilon eq} / K_{teq})}{\log(K_{teq} / K_{\sigma eq})} = 1.10$$

(2) **Cyclic loading**

K_{teq}, $K_{t\sigma}$ and K_{tm} are the same as for monotonic loading.

From the elastic-plastic analysis taken from Figure 9:

$K_{\sigma eq} = \Delta\hat{\sigma}_{eq} / \Delta\sigma_a = 1.8$, $K_{\varepsilon eq} = \Delta\hat{\varepsilon}^t_{eq} / \Delta\varepsilon_a = 4.04$

$K_{\sigma m} = \Delta\hat{\sigma}_m / \Delta\sigma_a = 2.38$, $K_{\varepsilon m} = \Delta\hat{\varepsilon}^t_m / \Delta\varepsilon_a = 4.02$

For meridional stress and strain using Equation 10:

$$m = \frac{\log(K_{\varepsilon m} / \alpha K_{tm})}{\log(K_{tm} / K_{\sigma m})}$$

where $\alpha K_{tm} = K_{tm}$
thus m= 1.15
For equivalent stress and strain using Equation 5:

$$m = \frac{\log(K_{\varepsilon eq} / K_{teq})}{\log(K_{teq} / K_{\sigma eq})} = 1.0$$

9 SUMMARY OF CONCLUSIONS:

The stress and strain characteristics of the spot-welded joint component under peel-tension loading conditions have been investigated experimentally, numerically and analytically. These results are important to designers in assessing the integrity and fatigue life of such components, in particular when subjected to low cycle fatigue. A fatigue crack initiation life prediction can then be obtained using either smooth specimen fatigue life data or other standard numerical relationships (e.g. Mason[20]-Coffin[21]).

The experimental strain readings and the three different spot-welded models presented in this paper have shown that the solid model (using six-sided, eight-noded solid elements to simulate the spot-weld) gives the best predictions. Also, by increasing the applied load, the strain values increased. This results in an increase in the degree of discrepancies between the finite element models and the corresponding experimental readings. The normal strain readings in the X-direction (normal to the direction of the load) for both experimental and solid model are twice those obtained in Y-direction. These are generally caused by the bending stress induced in the normal direction.

For the elastic analysis, K_t was found to be independent of geometric parameter d/t > 0.4 for a constant L/W and L/d. Similar results were obtained for L/W > 2.5 and for constant W/d and t/d. However, the geometric parameter W/L (i.e., changing the plate width) was found to have a significant effect on K_t.

The elastic-plastic analysis has shown that the steady-state maximum stress and total strain range depend on load and material hardening assumptions. Beyond yielding, an increase in the nominal load, λ, resulted in an increase the normalized total stain with a corresponding reduction in the normalized stress. Also, increasing the material hardening parameter, β, gave a reduction in the normalized strain coupled with an increase in the normalized stress. The maximum total strains for repeated loading are significantly less the corresponding values for monotonic loading. The strain range predictions are compared with estimates using NSSC rules and it is shown that for all cases, the linear rule provides the lower bound. However, the upper limit was found to be dependent on the loading condition. The Neuber rule with index 'm' set equal to unity is found to be generally realistic and provide conservative estimates for the spot-welded joint under peel-tension loading.

10 REFERENCES

[1] D. Radaj, "Hot spot stress concept for spot-welded joints", *Structural Design and crash*

worthiness of automobiles, Springer-Verlag, 149-170 (1987).
[2] P. C. Wang, H. T. Corton and F. V. Lawrence, "A fatigue life prediction method for tensile-shear spot welds", *SAE,* Paper no. 850279 (1985).
[3] F. V. Lawrence and P.C. Wang, and H. T. Corton, "An empirical method for estimating the fatigue resistance of tensile-shear spot-weld" *SAE,* Paper no. 830035 (1983).
[4] D. H. Orts, "Fatigue strength of spot-welds under joints in HSLA steel", *SAE, Paper no. 810355* (1981).
[5] J. M. Barson, J. A. Davidson and M. Fujimoto, "Fatigue behaviour of spot-welds under variable amplitude loading", *SAE,* Paper no. 850369 (1985).
[6] F. V. Lawrence, H. T. Corton and J. C. McMahon, *Final report to the American iron and steel institute on the improvement of steel spot-weld fatigue resistance* (1983).
[7] S. D. Sheppard and M. Strange, " Fatigue life estimation in resistance spot welds: initiation and early growth phase", *Fatigue fracture engineering material structures*, **15**, 531-549 (1992).
[8] M. G. Forrest, "A comparative analysis of laser and resistance spot welds", *Automotive body design and engineering*, IBEC '94 (1994).
[9] K. Pal and D. L. Cornin, " Static and dynamic characteristics of spot-welded sheet metal beams", *Vibration of mechanical systems and history of mechanical design*, DE-Vol. 63, ASME, 97-104 (1993).
[10] Y. Rui, R. S. Borsos, R. Gopalakrishnan, H. N. Agrawal and C. Rivard, "Fatigue life prediction method for multi-spot-welded structures", *SAE*, paper No. 930571, 33-42 (1993).
[11] S. D. Sheppard, "Estimation of fatigue propagation life in resistance spot welds", *American society for Testing and Materials*, Advances in fatigue lifetime predictive techniques: Second volume, ASTM STP 1211. M. R. Mitchell and R. W. Landgraf, Eds., Philadelphia, 169-185 (1993).
[12] K. Biswas, "Determining the fatigue properties of automotive sheet under cyclic loading", *Technische Mitteilungen Krupp* (English translation), 33-40 (1994).
[13] H. Neuber, "Theory of stress concentration for shear strained prismatical bodies with arbitrary nonlinear stress-strain law", *J. Applied Mech*., **28**, 544-550 (1961).
[14] H. F. Hardrath and L. Ohman, "A study of elastic and plastic stress concentration factors due to notches and fillets in flat plates", *NACA,* report 1117 (1953).
[15] H. O. Fuchs and R. I. Stephens, *Metal Fatigue in Engineering*, J. Wiley and Sons, N. Y. (1980).
[16] K. J. Miller and M. W. Brown, "Multiaxial fatigue"*, American Society for Testing and Materials*, ASTM STP 853, Philadelphia, Pa, 553-634 (1985).
[17] A.R. Gowhari-Anaraki, M. K. Pipelzadeh and S. J. Hardy, "Comparison between experiment and finite element models of spot-welded joints and assessment of their effect on elastic stress concentration factors", to be submitted to the *Journal of Strain Analysis* (2002).

[18] J. P. Caffrey and J. M. Lee, *MSC/NASTRAN linear static analysis user's guide*, The Macneal-Schwendler Corporation (1994).
[19] S. J. Hardy and A. R. Gowhari-Anaraki, "Stress concentration factors and elastic-plastic stress and strain predictions for axisymmetric internal projections on hollow tubes subjected to axial loading", *Journal of Strain Analysis*, **24**, 45-54 (1989).
[20] S. S. Manson, "Behaviour of materials under conditions of thermal stress", *NACA,* TN-2933 (1953).
[21] L. F. Jr. Coffin, "A study of the effect of cyclic thermal stresses on a ductile metal", *Trans. ASME*, **76**, 931-950 (1954).